Spin-squeezing-enhanced dual-species atom interferometric accelerometer employing large momentum transfer for precision test of the equivalence principle

Jinyang Li,[1] Gregório R. M. da Silva,[1] Schuyler Kain,[1] Jason Bonacum,[3] David D. Smith,[4] Timothy Kovachy,[1] and Selim M. Shahriar[2,3]

[1]*Department of Physics and Astronomy, Northwestern University, Evanston, Ilinois 60208, USA*
[2]*Department of Electrical and Computer Engineering, Northwestern University, Evanston, Illinois 60208, USA*
[3]*Digital Optics Technologies, Rolling Meadows, Illinois 60008, USA*
[4]*NASA Marshall Space Flight Center, Space Systems Department, ES23, Huntsville, Alabama 35812, USA*

(Received 20 February 2023; accepted 15 June 2023; published 7 July 2023)

We theoretically investigate the feasibility of applying spin squeezing to a light pulse atom interferometer in the presence of large momentum transfer using off resonant Raman transitions, in order to enhance the sensitivity of accelerometry close to the Heisenberg limit. We also show how to implement this scheme in a dual-species atom interferometer for a precision test of the equivalence principle by measuring the Eötvös parameter, and to identify the spin squeezing protocol that is best suited for such an experiment. For a space borne platform in low Earth orbit, such a scheme may eventually enable the measurement of the Eötvös parameter with a sensitivity of the order of 10^{-20} within 150 days when 10^5 atoms are employed in each cycle of the experiment.

DOI: 10.1103/PhysRevD.108.024011

I. INTRODUCTION

Precision test of the equivalence principle (EP), which lies at the heart of general relativity (GR), is one of the grand challenges in fundamental physics. The EP is characterized by the Eötvös parameter, η, which is defined as the ratio of the relative acceleration to the mean acceleration of two objects with different inertial masses under free fall in a gravitational field. GR has been immensely successful in predicting many phenomena. However, there are also reasons to believe that GR is incomplete. One indication of this is that GR cannot be reconciled with the standard model (SM). EP violation was found by the Committee on the Physics of the Universe to be relevant to four of the eleven questions that are the focus of the landmark study commissioned by the National Research Council [1]. Search for EP violation with ever increasing precision thus attempts to answer these four questions: Did Einstein have the last word on gravity? Are there additional space-time dimensions? What is the nature of dark energy? Is a new theory of matter and light needed at the highest energies?

Fundamentally, a violation of the EP arises when the SM is augmented by a new field with gravitational-strength coupling [2]. Since this field does not couple universally to SM fields, it causes different rates of fall. Such fields are explored in many theories, including those attempting to unify gravity with the other fundamental interactions. Proposals with concrete predictions for EP violation include Lorentz-violating fields introduced as part of the SM extension [3,4], cosmological models where a new field couples indirectly to SM fields via interactions with dark matter [5], chameleon fields with density dependent masses [6,7], and modified-gravity theories in which the new field is related to spacetime curvature [8].

The most precise test of the EP has been carried out under the satellite-borne MICROSCOPE experiment employing classical accelerometers [9,10]. The final result from this experiment [10] constrains the value of η to $\sim 1.5 \times 10^{-15}$. Efforts are underway to reach a sensitivity of 10^{-18} under the STEP experiment [11]. While it is predicted by some models that the extent of EP violation is on the order of $\eta \sim 10^{-18}$ [2], targeting higher measurement precision is necessary for two reasons. Firstly, the validity of these models cannot be guaranteed, suggesting the possibility of a lower degree of EP violation. Secondly, a more precise measurement of the degree of EP violation offers more information for the validity and accuracy of the theories. Here, we propose the use of space-borne dual species atomic interferometry, augmented by spin squeezing and large momentum transfer, that may make it possible to reach a sensitivity of $\eta < 10^{-20}$ within 150 days when 10^5 atoms are employed in each cycle of the experiment.

The conventional dual-species light pulse atom interferometer offers the potential to test the equivalence principle [12–21] and to search for the wavelike dark matter [22,23] with high precision. This approach has

constrained the value of η to 1.5×10^{-12} using a terrestrial experiment [13]. It has been estimated that a space-borne version of a similar experiment, employing five parallel dual species atom interferometers employing Bose-Einstein condensates, can reach a sensitivity to measure η as small as 10^{-17} in 18 months [24]. The technique of large momentum transfer (LMT) [25–34] has been used for enhancing the sensitivity of a dual-species atom interferometer [12,13]. However, another technique that can in principle enhance the sensitivity of the atom interferometer, namely spin squeezing [35–39], has not yet been applied to a dual-species atom interferometer. Furthermore, the combination of LMT and spin squeezing has not been investigated even for the single-species atom interferometer. It should also be noted that for atom interferometry, spin squeezing has only been used for suppressing the quantum projection noise [40,41], which reduces the resistance to detection noise. Alternative approaches of spin squeezing that produces phase magnification [42,43] to increase the resistance to detection noise has not been explored in the context of atomic interferometry.

In recent years, we have been investigating, separately, the use of LMT in atom interferometry [25] as well as the application of various protocols using cavity-induced one-axis-twist squeezing (OATS) for enhancing the sensitivity of atom interferometers and atomic clocks [42–45]. The approach for realizing OATS that has been studied most extensively, theoretically as well as experimentally, is the one based on cavity-mediated interactions [36–39]. In what follows, we consider, for specificity, only this approach for realizing the OATS scheme. The Hamiltonian of OATS can be expressed as $\hbar\chi S_z^2$, where S_z is the z component of collective spin operator, and χ is a characteristic frequency representing the squeezing process. The corresponding propagator can be expressed as $e^{-i\mu S_z^2}$, where μ is the squeezing parameter, defined as χ times the interaction time. Arguably the most promising approach for applying OATS to atomic interferometry makes use of the so-called generalized echo squeezing protocol (GESP) [42], which is predicted to yield a sensitivity of the Heisenberg limit divided by $\sqrt{2}$. The GESP has two versions. Their behavior does not differ much until μ approaches $\pi/2$. As μ approaches $\pi/2$, one version is optimized for even N, where N is the number of atoms and is thus denoted as GESP-e, while the other version is optimized for odd N, denoted as GESP-o. Other protocols of interest with similar degree of enhancement in sensitivity include the Schrödinger cat state protocol (SCSP) [42–44], and the conventional echo squeezing protocol (CESP) [46,47]. The SCSP also has two versions, namely SCSP-e and SCSP-o, where SCSP-e is optimized for even N, and SCSP-o is optimized for odd N. Both versions of the GESP become identical to the corresponding version of the SCSP for $\mu = \pi/2$. Each of the squeezing protocols mentioned above employs the squeezing operation and the inverse of the squeezing operation.

To apply OATS to the atom interferometer, we first need to determine whether the Raman pulse [48,49] or the Bragg pulse [31,34] should be used for the interferometer. In principle, two momentum states with the same internal state coupled by a Bragg transition can also be squeezed [50]. However, squeezing the momentum states using the OATS process may not work well for alkali atoms, mainly because the linewidths of optical transitions (∼6 MHz, for example, in Rb), relevant for the three-level system used in OATS, are much larger than the energy difference (∼15 kHz for Rb) between the two momentum states coupled by a Bragg transition. In contrast, the two ground states involved in the Raman transition is 3.0 GHz for ^{85}Rb and 6.8 GHz for ^{87}Rb, which are much larger than the linewidths of the optical transitions. Therefore, in this paper, we only consider atom interferometers employing Raman pulses.

In Refs. [42–44], we proposed the SCSP and the GESP versions of the squeezing protocols mentioned above, adapted to the atom interferometer. These versions are based on the conventional light pulse atom interferometer that uses counterpropagating Raman pulses in the sequence of $\pi/2$, π, $\pi/2$. However, these versions of the squeezing protocols have a practical problem. The distance between the two states of the atoms produced by the first $\pi/2$ pulse will keep increasing during the squeezing process, which imposes significant constraints on the squeezing operation, especially for protocols that require a relatively long atom-cavity interaction time. Therefore, in this paper we adopt a different scheme of atom interferometry that uses a hybrid of counterpropagating Raman pulses and copropagating Raman pulses [40,41]. Of course, the copropagating Raman pulses can be substituted with microwave pulses. For concreteness, we assume that only the counterpropagating Raman pulses and the microwave pulses would be used. In this paper, we describe how the SCSP and the GESP can be realized using this version of atom interferometry. In addition, we show how to augment these protocols to accommodate large momentum transfer (LMT).

It is not obvious whether a dual-species atom interferometer can adopt the technique of spin squeezing. One immediate problem of incorporating cavity-assisted OATS is that the two species must be squeezed individually to prevent entanglement between the two species but must be overlapped during the step of phase shift accumulation. In this paper, we also propose a scheme for a dual-species atom interferometer that employs both spin squeezing and LMT.

The rest of the paper is organized as follows. In Sec. II, we illustrate the experimental scheme and the sensitivity analysis for atom interferometer employing spin squeezing for acceleration sensing. In Sec. III, we discuss how to adapt the spin-squeezed atom interferometer to a dual-species atom interferometer for the EP test. The conclusion is given in Sec. IV.

II. SPIN-SQUEEZED ATOM INTERFEROMETER FOR ACCELERATION SENSING

In order to describe the LMT augmented and spin-squeezed atom interferometry protocols, we first introduce the notations of the relevant states. Each atom is modeled as a three-level system with the two ground states denoted as $|\pm\hat{\mathbf{z}}_0\rangle$ and the excited state denoted as $|e\rangle$. In practice, the two ground states are typically the $m_F = 0$ Zeeman substates of the two hyperfine ground states of an alkali atom. The microwave will couple these two ground states. The wavenumber of the beam coupling the state $|\pm\hat{\mathbf{z}}_0\rangle$ and $|e\rangle$ is denoted as $\boldsymbol{k}_\pm$. This three-level system can be reduced to a two-level system, with the effective wavenumber of the pair of counterpropagating Raman beams expressed as $\boldsymbol{k}_{\text{eff}} = (\boldsymbol{k}_+ - \boldsymbol{k}_-)$ if the direction of $\boldsymbol{k}_{\text{eff}}$ is defined to be that of $\boldsymbol{k}_+$. The absolute value of the effective wavenumber can be expressed as $k_{\text{eff}} = (k_+ + k_-) \approx 2k_+$, where $k_\pm$ is the absolute value of the corresponding wavenumber.

The two-level system can be modeled as spin-1/2 pseudo-spinors, with the spin operator defined as $\boldsymbol{s} = (s_x, s_y, s_z)$. In this notation, the subscripts $\{x, y, z\}$ represent the three dimensions of the Bloch sphere rather than dimensions of the physical space.

The five OATS-based protocols mentioned in the Introduction, namely SCSP-e, SCSP-o, GESP-e, GESP-o, and the CESP, all involve very similar sequences of pulses [42], and can be denoted as variations of the echo squeezing protocol (ESP). The differences are only the rotation axes of microwave pulses and the duration of the squeezing and unsqueezing pulses. Here, we describe specifically SCSP-e. Later on, we will discuss how the protocol can be modified easily to realize the GESP or the CESP protocols. Figure 1(a) shows the basic version of the pulse sequence of the echo squeezed atom interferometer where the momentum transfer is $2\hbar k_{\text{eff}}$ (in contrast to the conventional atom interferometer where the momentum transfer is $\hbar k_{\text{eff}}$). In this protocol, all microwave pulses cause rotations around the y axis. The pulse sequence of the protocol is as follows. The atoms are initially in state $|+\hat{\boldsymbol{z}}, 0\rangle$, which is a collective state where all the atoms are in state $|+\hat{\mathbf{z}}_0\rangle$ with a linear momentum of zero along the propagation direction of the Raman beams. Application of the first microwave $\pi/2$ pulse is followed by the OATS process with $\mu = \pi/2$, which produces the so-called x-directed Schrödinger cat state, defined as $(|+\hat{\mathbf{x}}, 0\rangle + e^{i\varphi}|-\hat{\mathbf{x}}, 0\rangle)/\sqrt{2}$. Here, φ is a phase resulting from the squeezing process. The OATS operation is followed by the second microwave $\pi/2$ pulse, which creates a z-directed Schrödinger cat state $(|-\hat{\mathbf{z}}, 0\rangle + e^{i(\varphi+\varphi')}|+\hat{\mathbf{z}}, 0\rangle)/\sqrt{2}$, where φ' is a phase resulting from this auxiliary rotation. It should be noted that the phase $\varphi + \varphi'$ is irrelevant and will be canceled during the inverse of the auxiliary rotation and the squeezing operation [51]. As such, for simplicity, we assume it to be zero. The first counterpropagating Raman π pulse (A_1) transforms $|\pm\hat{\mathbf{z}}, 0\rangle$ to $|\mp\hat{\mathbf{z}}, \pm\hbar k_{\text{eff}}\rangle$, resulting in beam splitting. Next, another Raman π pulse (B_{-1}) transforms $|\mp\hat{\mathbf{z}}, \pm\hbar k_{\text{eff}}\rangle$ to $|\pm\hat{\mathbf{z}}, 0\rangle$. This is followed by the application of a microwave π pulse, and then another Raman π pulse (B_1). After the application of the final Raman π pulse (C_{-1}), the state of the atoms can be expressed as $(|+\hat{\mathbf{z}}, 0\rangle + e^{iN\psi}|-\hat{\mathbf{z}}, 0\rangle)/\sqrt{2}$, where ψ is the acceleration-induced phase shift for a single atom. Pulse C_{-1} is followed by a $\pi/2$ microwave pulse that transforms the state to $(|+\hat{\mathbf{x}}, 0\rangle + e^{iN\psi}|-\hat{\mathbf{x}}, 0\rangle/)/\sqrt{2}$. Next, the application of the inverse of the OATS operation induces the interference between the upper arm and the lower arm, which produce the state $\cos(N\psi/2)|+\hat{\mathbf{x}}, 0\rangle + \sin(N\psi/2)|-\hat{\mathbf{x}}, 0\rangle$. The final microwave $\pi/2$ pulse rotates the state to $\cos(N\psi/2)|-\hat{\mathbf{z}}, 0\rangle + \sin(N\psi/2)|+\hat{\mathbf{z}}, 0\rangle$ so that the phase shift can be measured by detecting the population of state $|\pm\mathbf{z}_0\rangle$. We can see that the phase shift is magnified by a factor of N in this case. This is why the protocol stated above can enhance the sensitivity of an atom interferometer. Figure 1(b) shows the pulse sequences for the atom interferometer with a momentum transfer of $4\hbar k_{\text{eff}}$. The protocol shown in Fig. 1(b) contains four additional Raman π pulse A_2, B_{-2}, B_2, C_{-2}. Pulse A_2 transforms $|\mp\hat{\mathbf{z}}, \pm\hbar k_{\text{eff}}\rangle$ to $|\pm\hat{\mathbf{z}}, \pm 2\hbar k_{\text{eff}}\rangle$ and thus, increases the momentum transfer. The rest of the additional pulses are necessary for converging the two arms since they are separated farther away. This approach can be extended to produce even larger momentum transfer. For example, in Fig. 1(b), we illustrate the case where the momentum transfer is $6\hbar k_{\text{eff}}$.

The other protocols can be viewed as modifications of SCSP-e. In SCSP-o, all the microwave pulses except the first and the last ones are around the x axis. The steps in GESP-e(o) are the same as those in SCSP-e(o), except that the squeezing and unsqueezing interaction times are shorter, corresponding to $\mu < \pi/2$. Thus, GESP-e(o) becomes identical to SCSP-e(o) for $\mu = \pi/2$. The CESP differs from GESP-o only in the very last step, where the last microwave $\pi/2$ pulse causes a rotation around the x axis.

We next calculate the value of ψ, the acceleration-induced phase shift for a single atom. The propagator for a microwave $\pi/2$ pulse representing a rotation around the $x(y)$ axis can be expressed as $\exp[-i(\pi/2)s_{x(y)}]$. The effective Hamiltonian of the Raman pulse, which couples states differing in linear momenta by $\hbar k_{\text{eff}}$, can be expressed, in the absence of two-photon detuning, as

$$H = \frac{1}{2}\begin{bmatrix} 0 & -i\Omega e^{-i\phi} \\ i\Omega e^{i\phi} & 0 \end{bmatrix}, \tag{1}$$

where $\phi = \mathbf{k}_{\text{eff}} \cdot \mathbf{r} + \phi_0$ is the phase of the light field at the position of the atom, with ϕ_0 accounting for any additional phase difference between the Raman beat signal and the microwave field [45]. However, explicit knowledge of the value of ϕ_0 is not relevant, since it can be easily checked

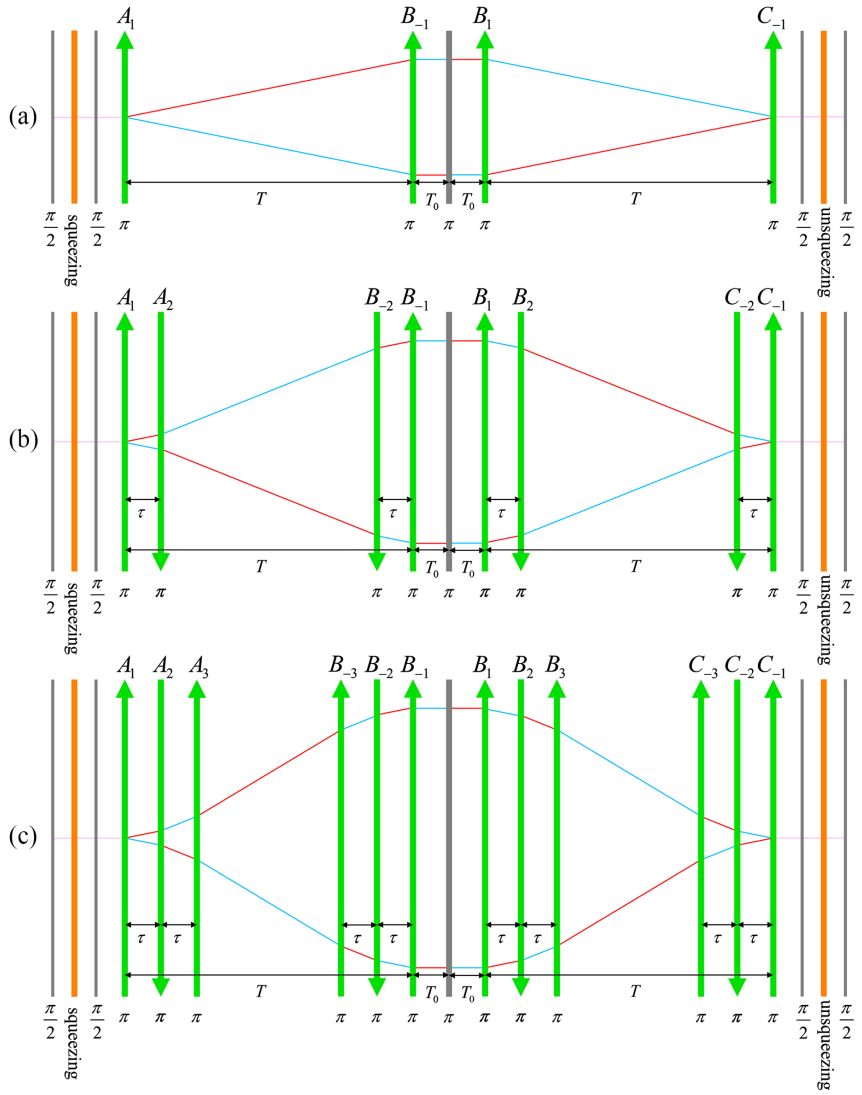

FIG. 1. Pulse sequences of (a) the basic version of the spin squeezing protocol for the atom interferometer with a momentum transfer of the spin squeezing protocol for the atom interferometer with a momentum transfer of $2\hbar k_{\text{eff}}$, (b) the spin squeezing protocol for the atom interferometer with a momentum transfer of $4\hbar k_{\text{eff}}$, (c) the spin squeezing protocol for the atom interferometer with a momentum transfer of $6\hbar k_{\text{eff}}$. The green arrows represent the Raman pulses, and the gray lines represent the microwave pulses. The blue (red) lines represent states $|\pm\hat{\mathbf{z}}_0\rangle$. The horizontal axis is time and the vertical axis corresponds to the physical vertical coordinate.

that it does not affect the signal in these protocols. Accordingly, in the following discussion, ϕ_0 is assumed to be zero. The corresponding propagators for the Raman π pulses can be expressed as

$$U_\pi = \begin{bmatrix} 0 & -e^{-i\phi} \\ e^{i\phi} & 0 \end{bmatrix} = e^{-i2\phi s_z} e^{-i\pi s_y} = e^{-i\pi s_y} e^{i2\phi s_z}, \quad (2)$$

which represents a rotation around $\hat{\mathbf{y}}\cos\phi - \hat{\mathbf{x}}\sin\phi$ on the Bloch sphere. It should be noted that these propagators only contain the linear terms of the spin operators in the exponent, so that the corresponding propagators for the ensemble can be obtained simply by replacing the single atom operators s_w $(w = x, y, z)$ with the collective spin operators S_w.

For concreteness, we first focus on GESP-e, in which all the pulses are around the y axis. With the propagator of a π pulse shown in Eq. (2), the net propagator for pulse A_1 and B_{-1} can be calculated to be

$$\begin{aligned}&(e^{-i2(\phi_{A_1}+\phi_0)S_z} e^{-i\pi S_x})(e^{-i\pi S_x} e^{i2(\phi_{B_{-1}}+\phi_0)S_z}) \\ &\quad = \pm e^{i2(\phi_{B_{-1}}-\phi_{A_1})S_z} = \pm e^{i2\mathbf{k}_{\text{eff}}\cdot(\mathbf{r}_{B_{-1}}-\mathbf{r}_{A_1})S_z}, \end{aligned} \quad (3)$$

where the sign $\pm$ represents $+(-)$ when the number of atoms is even (odd). However, this sign issue is irrelevant in this context. It can be seen from Eq. (3) that two consecutive π pulses is equivalent to a rotation around the

z axis on the Bloch sphere, with the rotation angle proportional to the displacement of the atoms between A_1 and B_{-1}. Similarly, the net propagator for pulse B_1 and C_{-1} is calculated to be $\pm e^{i2\mathbf{k}_{\mathrm{eff}}\cdot(\mathbf{r}_{C_{-1}}-\mathbf{r}_{B_1})S_z}$. Therefore, the equivalent propagator for the pulses between the squeezing and the unsqueezing operations can be calculated to be

$$\begin{aligned} & e^{-i(\pi/2)S_y} e^{i2\boldsymbol{k}_{\mathrm{eff}}\cdot(\boldsymbol{r}_{C_{-1}}-\boldsymbol{r}_{B_1})S_z} e^{-i\pi S_y} e^{i2\boldsymbol{k}_{\mathrm{eff}}\cdot(\boldsymbol{r}_{B_{-1}}-\boldsymbol{r}_{A_1})S_z} e^{-i(\pi/2)S_y} \\ & \quad = e^{-i(\pi/2)S_y} e^{i2\boldsymbol{k}_{\mathrm{eff}}\cdot(\boldsymbol{r}_{C_{-1}}-\boldsymbol{r}_{B_1})S_z} e^{-i2\boldsymbol{k}_{\mathrm{eff}}\cdot(\boldsymbol{r}_{B_{-1}}-\boldsymbol{r}_{A_1})S_z} \\ & \qquad \times e^{-i\pi S_y} e^{-i(\pi/2)S_y} \\ & \quad = e^{-i(\pi/2)S_y} e^{i2\boldsymbol{k}_{\mathrm{eff}}\cdot(\boldsymbol{r}_{A_1}-\boldsymbol{r}_{B_{-1}}-\boldsymbol{r}_{B_1}+\boldsymbol{r}_{C_{-1}})S_z} e^{-i(3\pi/2)S_y} \\ & \quad = \pm e^{-i2\boldsymbol{k}_{\mathrm{eff}}\cdot(\boldsymbol{r}_{A_1}-\boldsymbol{r}_{B_{-1}}-\boldsymbol{r}_{B_1}+\boldsymbol{r}_{C_{-1}})S_x}, \end{aligned} \tag{4}$$

which is a rotation around the x axis on the Bloch sphere. The step from the first line to the second line in Eq. (4) makes use of the relation shown in Eq. (2). Here, we have assumed that there is no Sagnac effect induced phase shift due to rotation. We can see that the net effect of the pulses between the squeezing and the unsqueezing process is only a rotation around the x axis on the Bloch sphere by an angle of the phase shift. Therefore, it can be seen that the protocol shown in Fig. 1(a) is equivalent to the fundamental three-step GESP-e described in Ref. [42], with the phase shift $\psi = 2\boldsymbol{k}_{\mathrm{eff}}\cdot(\boldsymbol{r}_{A_1}-\boldsymbol{r}_{B_{-1}}-\boldsymbol{r}_{B_1}+\boldsymbol{r}_{C_{-1}})$, which is calculated to be $2\boldsymbol{k}_{\mathrm{eff}}\cdot\boldsymbol{a}(T^2+2TT_0)$, where the time intervals T and T_0 are as defined in Fig. 1(a). Accordingly, this basic version of GESP-e augmented atom interferometer can be used for accelerometry. It should be noted that in the case of $\mu=\pi/2$, for which GESP-e becomes the same as SCSP-e, this phase gets magnified by a factor of N, as shown earlier. When the concomitant increase of the quantum noise by a factor of $\sqrt{N}$ is considered, the sensitivity reaches the Heisenberg limit.

Consider next the atom interferometer augmented with both the GESP and LMT, corresponding to the cases shown in Figs. 1(b) and 1(c). In this case, the only difference is that the phase shift becomes $\boldsymbol{k}_{\mathrm{eff}}\cdot[\sum_{j=1}^{n}(\boldsymbol{r}_{A_j}-\boldsymbol{r}_{B_{-j}}-\boldsymbol{r}_{B_j}+\boldsymbol{r}_{C_{-j}})]$, where n is the factor by which the momentum splitting is augmented using the LMT process [e.g., $n=3$ if the momentum splitting is $6\hbar k_{\mathrm{eff}}$, corresponding to the case shown in Fig. 1(c)]. It can be shown that the phase shift can be expressed as $\psi = 2n\boldsymbol{k}_{\mathrm{eff}}\cdot\boldsymbol{a}[T^2+2TT_0-(n-1)T\tau]$, where the time interval τ is as defined in Figs. 1(b) and 1(c). For $T\gg\tau$, the acceleration phase shift can be approximated as $2n\boldsymbol{k}_{\mathrm{eff}}\cdot\boldsymbol{a}(T^2+2TT_0)$. Therefore, the spin-squeezed atom interferometer with LMT magnifies the phase shift by a factor of $2n$ compared to the conventional $\pi/2$-π-$\pi/2$ interferometer and thus, enhances the sensitivity by a factor of $2n$, if the noise and the signal amplitude reduction caused by LMT are negligible.

The primary effect of all squeezing protocols considered above is to increase the gradient of the signal with respect to the phase shift, $|\partial\langle S_z\rangle/\partial\psi|$, where S_z is the quantum operator measured [42–44]. The SCSP magnifies the phase gradient by a factor of N if the parity of N matches the version of the SCSP but also increases the quantum noise by a factor of $\sqrt{N}$ [44]. Therefore, the SCSP can reach the Heisenberg limit for a known parity of N. Taking into account the application of LMT, the sensitivity is totally enhanced by a factor of $2n\sqrt{N}$, compared to the conventional $\pi/2$-π-$\pi/2$ interferometer. Both versions of the GESP work optimally in the interval $4\sqrt{2/N}\le\mu\le\pi/2-\sqrt{2/N}$. In this interval, the phase gradient is magnified by a factor of $N\sin\mu/\sqrt{2}$, and the quantum noise is amplified by factor of $\sqrt{N/2}\sin\mu$. Therefore, the ideal sensitivity is enhanced by a factor of $\sqrt{N/2}$, reaching the Heisenberg limit divided by $\sqrt{2}$. Taking into account the application of LMT, the sensitivity is totally enhanced by a factor of $n\sqrt{2N}$, compared to the conventional $\pi/2$-π-$\pi/2$ interferometer. The CESP is optimal only for $\mu=N^{-1/2}$. With this value of μ, the phase gradient is magnified by a factor of $\sqrt{N/e}$, while the quantum noise is not changed. Accordingly, the ideal sensitivity reaches the Heisenberg limit divided by $\sqrt{e}$. Again, taking into account the application of LMT, the sensitivity is totally enhanced by a factor of $2n\sqrt{N/e}$, compared to the conventional $\pi/2$-π-$\pi/2$ interferometer. Although ideally all these ESPs can approach the Heisenberg limit, their actual sensitivities in the absence in the presence of detection noise and decoherence mechanisms can differ a lot. The SCSP is robust against detection noise but vulnerable to decoherence mechanisms, while the CESP is less robust against detection noise but more resistant to decoherence mechanisms. The GESP can balance the properties of these two protocols and is thus possibly the most promising ESP [42].

III. SCHEME FOR TESTING THE EQUIVALENCE PRINCIPLE

A dual-species atom interferometer can be used to test the equivalence principle [12,13]. In such an interferometer, the two isotopes are initially captured in the same magneto-optic trap. So far, Bragg pulses have been used in dual-species atom interferometers employing ^{87}Rb and ^{85}Rb because a single pair of Bragg beams can address both isotopes. In this way, the effective wavenumber of the Bragg beams, k_{eff}, and the half duration of the interferometer sequence, T, are naturally the same for both isotopes. Therefore, the acceleration phase shift $k_{\mathrm{eff}}aT^2$ only depends on the acceleration a for both isotopes.

In principle, Raman pulses can also be used for such a dual-species atom interferometer. However, two different pairs of monochromatic Raman beams are needed to

address the two isotopes. These two pairs of Raman beams can be combined and controlled with the same switch so that they spatially coincide and are exactly synchronized. To make the value of k_{eff} the same for the two pairs of Raman beams, we can produce them from the same laser. To produce the Raman beams for ^{85}Rb, we can guide a beam from the laser through an EOM (electro-optic modulator) tuned to ∼1.5 GHz, which is half the hyperfine splitting of the ground state. In this way, the $+1$ order and -1 order in the output of the EOM would differ in frequency by the hyperfine splitting, and their average value is the laser frequency. Each of these frequency components can be extracted with a Fabry-Perot cavity. Alternatively, two different AOMs (acousto-optic modulators) can be used for generating these frequency components, with one up-shifted and another down-shifted. The pair of counterpropagating Raman beams prepared using either approach would have a k_{eff} that is exactly twice the laser wavenumber. If the Raman beams for ^{87}Rb are prepared in the same way, their k_{eff} will equal the k_{eff} of the Raman beams for ^{85}Rb. Of course, it would be necessary to adjust the intensities of the beams to balance the light shifts [52] and make the effective Rabi frequencies for the two isotopes equal.

OATS is realized via nonlinear interaction between the atoms and the light in an optical cavity [36–39]. To ensure that the value of the single-photon Rabi frequency remains as uniform as possible longitudinally, it is preferable to use a ring cavity. In the model describing the mechanism of OATS, an atom is considered as a three-level system consisting of two ground states, denoted as $|\pm\hat{\mathbf{z}}_0\rangle$, and an excited state, denoted as $|e\rangle$, as discussed earlier. Ideally, to balance the light shifts of states $|+\hat{\mathbf{z}}_0\rangle$ and $|-\hat{\mathbf{z}}_0\rangle$, the cavity should be tuned to the average frequency of the transitions from $|+\hat{\mathbf{z}}_0\rangle$ to $|-\hat{\mathbf{z}}_0\rangle$ and from $|-\hat{\mathbf{z}}_0\rangle$ to $|e\rangle$ if we assume that the Rabi frequencies of these two transitions are the same. In practice, the states $|+\hat{\mathbf{z}}_0\rangle$ and $|-\hat{\mathbf{z}}_0\rangle$ are, respectively, the $F=3$, $m_F=0$ ($F=2$,$m_F=0$) and $F=2$, $m_F=0$ ($F=1$, $m_F=0$) Zeeman substates for the case of ^{85}Rb (^{87}Rb), state $|e\rangle$ is the $5P_{3/2}$ manifold, which contains multiple hyperfine states, and the probe beam would be $\sigma^{\pm}$ polarized. Thus, it is necessary to augment the model to take into account the multiplicity of the hyperfine states in the $5P_{3/2}$ manifolds, and the coupling strengths between $|\pm\hat{\mathbf{z}}_0\rangle$ and the relevant Zeeman substates within the hyperfine states in the $5P_{3/2}$ manifold, in order to determine the optimal cavity resonance for each isotope. This analysis is summarized in the Appendix.

If the atoms of both isotopes are present in the cavity simultaneously during the OATS operation, the nonlinear interaction would produce entanglement among the atoms from both isotopes. As such, the OATS operation for the two isotopes must be carried out separately with two distinct cavities. In describing the process for the dual species atom interferometry augmented by the GESP and LMT, we refer to the steps illustrated earlier in Fig. 1. The protocol will start as follows. Atoms for each isotope would be trapped in a separate magneto-optic trap, followed by polarization gradient cooling and evaporative cooling. Each ensemble will then be loaded into a separate dipole force trap, which would be shifted spatially from each other along the direction of propagation of the Raman pump beams. The first microwave $\pi/2$ pulse, followed by the application of OATS and the auxiliary microwave $\pi/2$ pulse will all be carried out while the atoms are still in the dipole force traps. After this, the traps will be turned off, and the two ensembles will be overlapped by controlling the movement of one isotope, using the process described next.

Controlling the movement of one isotope can be realized with low-Rabi-frequency Raman transitions, as illustrated schematically in Fig. 2. When the dipole traps are turned off, the atoms are in a superposition of state $|+\hat{\mathbf{z}}_0, 0\rangle$ and $|-\hat{\mathbf{z}}_0, 0\rangle$. One method to impart a momentum to both states of ^{85}Rb is to apply a species-selective Raman π pulse consisting of two pairs of Raman beams, with one pair resonant with the transition from $|+\hat{\mathbf{z}}_0, 0\rangle$ to $|-\hat{\mathbf{z}}_0, \hbar k_{\text{eff}}\rangle$, and the other pair resonant with the transition from $|-\hat{\mathbf{z}}_0, 0\rangle$ to $|+\hat{\mathbf{z}}_0, \hbar k_{\text{eff}}\rangle$, as shown in Fig. 2(a). Unfortunately, such a Raman π pulse can have a side effect. Consider, for example, the pair of Raman beams that couples $|+\hat{\mathbf{z}}_0, 0\rangle$ to $|-\hat{\mathbf{z}}_0, \hbar k_{\text{eff}}\rangle$. Normally, this pair of Raman beams can also drive the undesirable transition from $|-\hat{\mathbf{z}}_0, 0\rangle$ to $|+\hat{\mathbf{z}}_0, -\hbar k_{\text{eff}}\rangle$. However, this side effect can be suppressed by noting that this Raman pulse is detuned from this undesirable transition by $\hbar k_{\text{eff}}^2/m \approx 30$ kHz (m is the mass of ^{85}Rb), as shown in Fig. 2(b). Therefore, if the effective Rabi frequency of the Raman pulse is much lower than 30 kHz, this Raman pulse will only impart to state $|+\hat{\mathbf{z}}_0, 0\rangle$ a momentum of $\hbar k_{\text{eff}}$. Of course, this method requires that the Doppler broadening of the counterpropagating Raman excitation is much less than 30 kHz, which is necessary anyway for such an experiment [13]. When the two isotopes overlap, the motion of the ^{85}Rb atoms is halted with another Raman π pulse identical to the one applied previously. The two Raman π pulses and the motion of the atoms controlled by them are shown in Fig. 2(c).

To find the effective Rabi frequency of the Raman pulse that should be used, we have implemented a numerical simulation of the efficiencies of the transition from $|+\hat{\mathbf{z}}_0, 0\rangle$ to $|-\hat{\mathbf{z}}_0, \hbar k_{\text{eff}}\rangle$ and the transition from $|-\hat{\mathbf{z}}_0, 0\rangle$ and $|+\hat{\mathbf{z}}_0, -\hbar k_{\text{eff}}\rangle$. The temperature of the atoms used for the simulation is 10 pK, which is the temperature of atoms in the equivalence-principle-test experiment reported in Ref. [24]. The corresponding Doppler broadening (standard deviation) of 10 pK Rb atoms is ∼80 Hz. Using a Blackman pulse envelope [53,54] instead of a square envelope can also suppress the undesired transition from $|-\hat{\mathbf{z}}_0, 0\rangle$ and $|+\hat{\mathbf{z}}_0, -\hbar k_{\text{eff}}\rangle$ due to the absence of the side

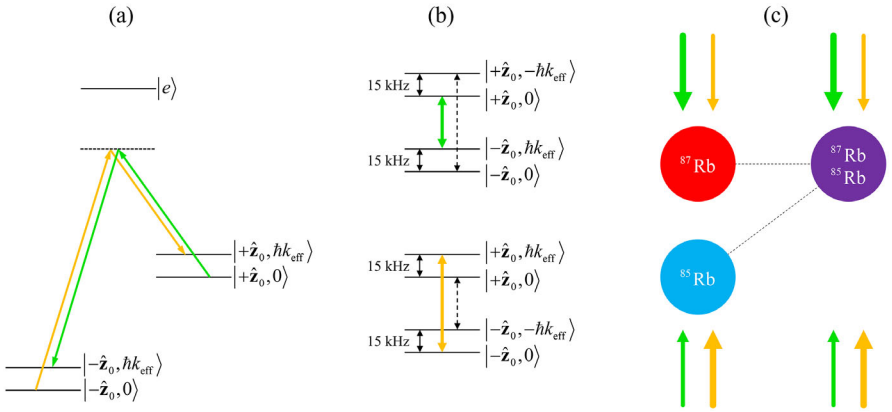

FIG. 2. Schematic illustration of the method to overlap the two isotopes. All Raman beams only address ^{85}Rb. (a) Raman transitions driven by the Raman π pulse consisting of two pairs of Raman beams. One pair is resonant with the transition from $|+\hat{\mathbf{z}}_0, 0\rangle$ to $|-\hat{\mathbf{z}}_0, \hbar k_{\rm eff}\rangle$ (green arrows), and the other pair is resonant with the transition from $|-\hat{\mathbf{z}}_0, 0\rangle$ to $|+\hat{\mathbf{z}}_0, \hbar k_{\rm eff}\rangle$ (orange arrows). (b) Illustration of transitions driven by the beat notes of the two pairs of Raman beams. The lengths of the green and oranges arrow indicate the frequencies of the beat notes. The resonant transitions in this diagram correspond to the ones shown in panel (a). In addition, other relevant neighboring energy levels are also shown here. The dashed lines indicate the possible but undesirable transitions in the presence of the Raman beams. As can be seen, the Raman beat notes are detuned from these transitions by 30 kHz, which sets limits on the maximum Raman Rabi frequency and the maximum temperature of the atoms. (c) Application of the two Raman π pulses and the motion of the atoms controlled by them. For each color, the thick (thin) arrows represent the Raman beam corresponding to the higher (lower) frequency leg. The first Raman π pulse imparts to the ^{85}Rb atoms a momentum of $\hbar k_{\rm eff}$ in the vertical direction. When they overlap the cloud of ^{87}Rb, the second Raman π pulse is applied to reverse the transitions, thus halting the motion of ^{85}Rb atoms in the vertical direction.

bumps in the Fourier spectrum. Actually, the power of a Blackman pulse is even more concentrated around the central frequency than a Gaussian pulse. The instant Rabi frequency of a Blackman π pulse is defined as

$$\Omega(t)=\begin{cases}\frac{\Omega_{\rm eff}}{0.84}(0.42+0.5\cos\frac{\pi t}{\tau_{\rm eff}}+0.08\cos\frac{2\pi t}{\tau_{\rm eff}}), & -\tau_{\rm eff}\le t\le\tau_{\rm eff}\\ 0, & \text{otherwise}\end{cases} \tag{5}$$

where $\Omega_{\rm eff}$ and $\tau_{\rm eff}$ are defined in such a way that $\int_{-\infty}^{\infty}\Omega(t)dt=\Omega_{\rm eff}\tau_{\rm eff}$. Therefore, a Blackman pulse is a π pulse if $\Omega_{\rm eff}\tau_{\rm eff}=\pi$.

The efficiencies of the two transitions as functions of $\Omega_{\rm eff}$ are shown in Fig. 3. The red curve shows the efficiency of the desirable transition from $|+\hat{\mathbf{z}}_0, 0\rangle$ to $|-\hat{\mathbf{z}}_0, \hbar k_{\rm eff}\rangle$, and the blue curve the undesirable transition from $|-\hat{\mathbf{z}}_0, 0\rangle$ to $|+\hat{\mathbf{z}}_0, -\hbar k_{\rm eff}\rangle$. We can see that the efficiency of the desired transition is $\sim$1 and the undesirable transition $\sim$0 if $\Omega_{\rm eff}$ is between 1 kHz to 10 kHz. Therefore, this technique to control the movement of one isotope is theoretically feasible. In addition, the technique described in Ref. [12] can suppress the remaining imperfection in the overlap between the two isotopes. After the antiauxiliary microwave $\pi/2$ pulse which appears before the unsqueezing pulse, we need to separate the two isotopes. The technique of low-Rabi-frequency Raman transition can still be used for such a purpose. Once the two isotopes are spatially separated, they can be confined in two dipole traps again and undergo the rest of the protocol, namely the unsqueezing process and the last microwave $\pi/2$ pulse.

Practically, it is difficult to make the values of μ for ^{85}Rb and for ^{87}Rb the same. The sensitivity of the spin squeezing protocols depends on the value of μ and the number of atoms, which will be generally different for these two isotopes. However, a very important aspect of the GESP protocol is that it has essentially the same sensitivity of the Heisenberg limit divided by $\sqrt{2}$ for a wide range of μ [42] and thus, is best suited for such a dual-species interferometer.

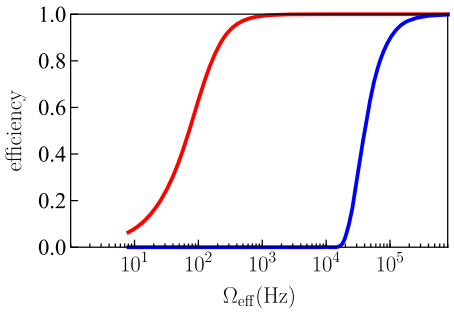

FIG. 3. Efficiencies of the two transitions as functions of $\Omega_{\rm eff}$ driven by a Blackman pulse. The red curve shows efficiency of the desirable transition from $|+\hat{\mathbf{z}}_0, 0\rangle$ to $|-\hat{\mathbf{z}}_0, \hbar k_{\rm eff}\rangle$, and the blue curve the undesirable transition from $|-\hat{\mathbf{z}}_0, 0\rangle$ to $|+\hat{\mathbf{z}}_0, -\hbar k_{\rm eff}\rangle$. We can see that the efficiency of the desired transition is $\sim$1 and the undesirable transition $\sim$0 if $\Omega_{\rm eff}$ is between 1 kHz to 10 kHz.

By modulating the phase of any one of the π pulses, denoted as ϕ_p, we can obtain the signal (namely, the difference between the population of $|+\hat{\mathbf{z}}_0\rangle$ state and the population of $|-\hat{\mathbf{z}}_0\rangle$ state) versus the phase shift. The total phase shift is $2nk_{\text{eff}}aT^2 + \phi_p$. Although the sensitivity can be made the same for these two isotopes, the widths of the fringes as a function of ϕ_p depend on the value of μ and the number of atoms. Assuming, for example, that the value of μ would be larger for ^{85}Rb, and the number of atoms trapped for ^{85}Rb would be higher, the fringes for ^{85}Rb would be narrower. If the equivalence principle holds, the central peaks, which correspond to the point where $2nk_{\text{eff}}aT^2 + \phi_p = 0$, will coincide, as shown in Fig. 4. Therefore, we can lock ϕ_p to the central peak (i.e., $\phi_p = -2nk_{\text{eff}}aT^2$) of one isotope and check whether the signal of the other isotope deviates from its central peak.

Ideally, the sensitivity of the GESP can be expressed as $2nk_{\text{eff}}\Delta aT^2 = \sqrt{2}/N$, where N is the number of atoms during the interrogation time, and Δa is the uncertainty of the measured relative acceleration. For $n = 5$, $T = 1$ s, and $N = 10^5$, which are close to the values of the parameters adopted in Ref. [13], the value of Δa is calculated to be 8.7×10^{-14} m $\cdot$ s^{-2}. If the experiment is implemented on the ground or in a low earth orbit, the gravitational acceleration is $\sim$9.8 m $\cdot$ s^{-2}. Therefore, the relative precision that can be achieved is $\eta = \Delta a/a = 8.8 \times 10^{-15}$ per shot, which is 1600 times the sensitivity reported in Ref. [13]. Of course, the experimental sensitivity reported in Ref. [13] did not reach the standard quantum limit. Compared to the theoretically highest sensitivity of the experiment in Ref. [13], which is the standard quantum limit, the factor of sensitivity enhancement would be $\sqrt{N/2} \approx 220$. It should also be possible to increase the number of atoms by a factor of 10 compared to what was employed in Ref. [13]. In that case, the sensitivity that can be achieved in a single shot would be $\eta = \Delta a/a = 8.8 \times 10^{-16}$, since the sensitivity under the GESP is proportional to N. If the experiment is implemented on a space-borne platform in a low earth orbit, the value of T can be much larger due to the weightless environment. If $T = 100$ s, which is reasonable for the temperature of the atoms envisioned above, and 10^5 shots are implemented, the ideally achievable sensitivity would be $\sim 2.8 \times 10^{-22}$. Taking into consideration that the state preparation takes up to 30 s [13,24], the duration of such a measurement is calculated to be $\sim$150 days.

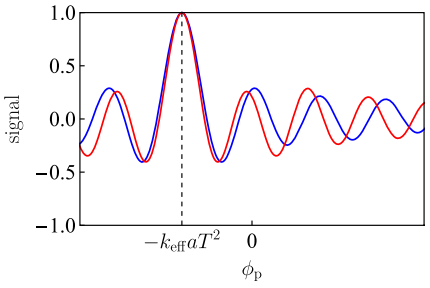

FIG. 4. Example of the signals of the generalized echo squeezing protocol for ^{85}Rb (red) and ^{87}Rb (blue). The position of the central peak is at $\phi_p = -k_{\text{eff}}aT^2$. If the equivalence principle holds, the central peaks of both isotopes will coincide.

Of course, in practice it would be exceedingly difficult to reach this ideal limit. As we have discussed at length in Ref. [42], the GESP makes it possible to reach the Heisenberg limit of sensitivity divided by $\sqrt{2}$ for a broad range of values of the squeezing parameter. The optimal choice of the squeezing parameter μ would depend on various sources of noise as well as decoherence mechanisms. As μ increases, the protocol is more robust against detection noise but more vulnerable to decoherence mechanisms, including cavity decay, residual spontaneous emission, and collisions between the atoms and background particles. A cavity with a high single-atom cooperativity could suppress the effect of cavity decay and residual spontaneous emission [42]. The single-atom cooperativity can be increased by shrinking the cavity mode as well as enhancing the quality factor. Meanwhile, a cryogenic vacuum [55] could significantly lower the rate of collisions with background particles. Assuming the use of a cavity with high single-atom cooperativity and a cryogenic vacuum, and operation of the GESP for the optimal value of μ, it might be possible to limit the ratio of the ideal sensitivity to the actual one within 36, which corresponds to an actual sensitivity on the order of $\sim 10^{-20}$. Of course, the number of shots can be increased to improve the sensitivity further. We would also like to note that the analysis of the effects of various sources of noise as presented in Ref. [42] is not comprehensive, and more detailed studies, theoretical as well experimental, are warranted in order to determine the actual degree of enhancement in sensitivity that could be achieved using the GESP in general, and the dual-species atomic interferometry augmented by LMT and the GESP in particular.

Increasing either the interrogation time or the momentum transfer can enhance the sensitivity. However, for an experiment even in the weightless environment, the length of the vacuum chamber l imposes a constraint $2n\hbar k_{\text{eff}}T/m \leq l$ because the two arms of the interferometer move apart at a relative velocity of $2n\hbar k_{\text{eff}}/m$. Recalling that the phase shift is $\phi = 2nk_{\text{eff}}aT^2$, we find that $\phi \leq malT/\hbar$, which is proportional to T but does not depend on n. Therefore, if the physical dimension of the apparatus is the primary constraint, it may be optimal to increase T at the expense of decreasing n, while satisfying the constraint $2n\hbar k_{\text{eff}}T/m \leq l$. However, other factors may restrict the maximum value of, T such as the expansion of the atomic cloud and long-term stability of the system. Taking these factors into account, the use of LMT is

expected to be useful for increasing the sensitivity of the experiment.

IV. CONCLUSION

We have shown theoretically the feasibility of applying spin squeezing to a light pulse atom interferometer even in the presence of large momentum transfer using off resonant Raman transitions, in order to enhance the sensitivity of accelerometry close to the Heisenberg limit. Even if practical imperfections lower the sensitivity from the ideal level, there is still a good chance to significantly surpass the standard quantum limit with this scheme. We also show how to implement this scheme in a dual-species atom interferometer for a precision test of the equivalence principle by measuring the Eötvös parameter. Based on experimental constraints, we find that the generalized echo squeezing protocol, which enhances the sensitivity close to the Heisenberg limit for a very broad range of values of the squeezing parameter, is the best suited for such an experiment. For a space borne platform in low Earth orbit, employing a cavity with a high single-atom cooperativity and a cryogenic vacuum system, such a scheme may enable the measurement of the Eötvös parameter with a sensitivity of the order of 10^{-20} within 150 days when 10^5 atoms are employed in each cycle of the experiment.

ACKNOWLEDGMENTS

This work has been supported equally in parts by NASA Grant No. 80NSSC20C0161, the Department of Defense Center of Excellence in Advanced Quantum Sensing under Army Research Office Grant No. W911NF202076, ONR Grant No. N00014-19-1-2181, and the U.S. Department of Energy, Office of Science, National Quantum Information Science Research Centers, Superconducting Quantum Materials and Systems Center (SQMS) under Contract No. DE-AC02-07CH11359.

APPENDIX: CALCULATION OF THE OPTIMAL CAVITY RESONANT FREQUENCY

In this appendix, we calculate the optimal cavity resonant frequency that balances the light shifts of the two ground hyperfine states of Rb. Specifically, we assume that the cavity field would be σ^+ polarized. We use first ^{87}Rb as the example to illustrate the calculation and then show what the result would be for ^{85}Rb. Consider first the light shift of the ground state $F = 2$, $m_F = 0$. The light field inside the cavity couples this state to the $m_F = 1$ Zeeman substate of each hyperfine state in the $5P_{3/2}$ manifold. Each coupling contributes a light shift to the ground state $F = 2$, $m_F = 0$.

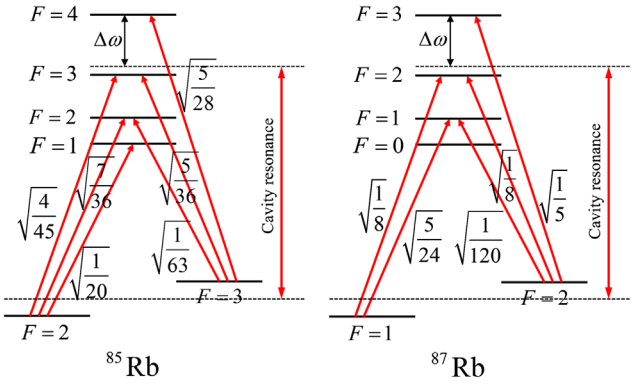

FIG. 5. Relevant transitions for calculating the optimal cavity resonance that balance the light shifts of the two ground states.

Therefore, the total light shift of this ground state is the sum of the light shifts by all the couplings, which can be expressed as

$$\omega_{\mathrm{LS2}} = \sum_{j=1}^{3} \frac{|\Omega_{2\to j}|^2}{4(\omega_{\mathrm{HFS}}/2 + \omega_{j3} - \Delta\omega)} = \Gamma^2 \sum_{j=1}^{3} \frac{|\alpha_{2\to j}|^2}{4(\omega_{\mathrm{HFS}}/2 + \omega_{j3} - \Delta\omega)}, \tag{A1}$$

where $\Omega_{2\to j}$ is the Rabi frequency of the transition from the ground state $F = 2$, $m_F = 0$ to the excited state $F = j$, $m_F = 1$, ω_{HFS} is the energy difference between the $F = 1$ and $F = 2$ states, ω_{j3} is the energy difference between $F = j$ ($j = 1, 2, 3$) and $F = 3$ in the $5P_{3/2}$ manifold, $\Delta\omega$ (whose optimal value is to be determined by this analysis) is as defined in Fig. 5, Γ is the spontaneous decay rate of the $5P_{3/2}$ manifold, and $\alpha_{2\to j}$ is the matrix element for the transition from the ground state $F = 2$, $m_F = 0$ to the excited state $F = j$, $m_F = 1$, as shown in Fig. 5. In this model, we have assumed that the Rabi frequency of the strongest transition remains much smaller than $\omega_{\mathrm{HFS}}/2$. A similar expression is used to determine the total light shift of the ground state $F = 1$, $m_F = 0$, denoted as ω_{LS1}. To balance the light shifts, we require that $\omega_{\mathrm{LS1}} + \omega_{\mathrm{LS2}} = 0$. Solving this equation, we can obtain the optimal value of $\Delta\omega$, which is $2\pi \times 235.7$ MHz for ^{87}Rb. It is important to note that this value is independent of the intensity of the probe field, as long the assumption regarding the Rabi frequency of the strongest transition stated above remains valid. Implementing the same calculation, we can also obtain the value of $\Delta\omega$ for ^{85}Rb, which is $2\pi \times 114.2$ MHz.

[1] NRC Committee on the Physics of the Universe (Chair, M. Turner) report Connecting Quarks with the Cosmos: Eleven Science Questions for the New Century, 2003, https://nap.nationalacademies.org/login.php?record_id=10079.

[2] J. Overduin, F. Everitt, P. Worden, and J. Mester, STEP and fundamental physics, Classical Quantum Gravity **29**, 184012 (2012).

[3] V. A. Kostelecky and J. D. Tasson, Prospects for Large Relativity Violations in Matter-Gravity Couplings, Phys. Rev. Lett. **102**, 010402 (2009).

[4] V. A. Kostelecky and J. D. Tasson, Matter–gravity couplings and Lorentz violation, Phys. Rev. D **83**, 016013 (2010).

[5] S. M. Carroll, S. Mantry, and M. J. Ramsey-Musolf, Implications of a scalar dark force for terrestrial experiments, Phys. Rev. D **81**, 063507 (2009).

[6] J. Khoury and A. Weltman, Chameleon Fields: Awaiting Surprises for Tests of Gravity in Space, Phys. Rev. Lett. **93**, 171104 (2004).

[7] D. F. Mota and D. J. Shaw, Evading equivalence principle violations, cosmological and other experimental constraints in scalar field theories with a strong coupling to matter, Phys. Rev. D **75**, 063501 (2007).

[8] S. Capozziello and S. Tsujikawa, Solar system and equivalence principle constraints on $f(R)$ gravity by the chameleon approach, Phys. Rev. D **77**, 107501 (2008).

[9] Pierre Touboul *et al.*, Space test of the equivalence principle: first results of the MICROSCOPE mission, Classical Quantum Gravity **36**, 225006 (2019).

[10] Pierre Touboul *et al.*, MICROSCOPE Mission: Final Results of the Test of the Equivalence Principle, Phys. Rev. Lett. **129**, 121102 (2022).

[11] The Satellite Test of the Equivalence Principle (STEP), http://einstein.stanford.edu/STEP/.

[12] C. Overstreet, P. Asenbaum, T. Kovachy, R. Notermans, J. M. Hogan, and M. A. Kasevich, Effective Inertial Frame in an Atom Interferometric Test of the Equivalence Principle, Phys. Rev. Lett. **120**, 183604 (2018).

[13] P. Asenbaum, C. Overstreet, M. Kim, J. Curti, and M. A. Kasevich, Atom-Interferometric Test of the Equivalence Principle at the 10^{-12} Level, Phys. Rev. Lett. **125**, 191101 (2020).

[14] S. Fray, C. A. Diez, T. W. Hänsch, and M. Weitz, Atomic Interferometer with Amplitude Gratings of Light and its Applications to Atom Based Tests of the Equivalence Principle, Phys. Rev. Lett. **93**, 240404 (2004).

[15] A. Bonnin, N. Zahzam, Y. Bidel, and A. Bresson, Simultaneous dual-species matter-wave accelerometer, Phys. Rev. A **88**, 043615 (2013).

[16] D. Schlippert, J. Hartwig, H. Albers, L. L. Richardson, C. Schubert, A. Roura, W. P. SchleichW. Ertmer, and E. M. Rasel, Quantum Test of the Universality of Free Fall, Phys. Rev. Lett. **112**, 203002 (2014).

[17] M. G. Tarallo, T. Mazzoni, N. Poli, D. V. Sutyrin, X. Zhang, and G. M. Tino, Test of Einstein Equivalence Principle for 0-Spin and Half-Integer-Spin atoms: Search for Spin-Gravity Coupling Effects, Phys. Rev. Lett. **113**, 023005 (2014).

[18] L. Zhou *et al.*, Test of Equivalence Principle at 10^{-8} Level by a Dual-Species Double-Diffraction Raman Atom Interferometer, Phys. Rev. Lett. **115**, 013004 (2015).

[19] B. Barrett, L. Antoni-Micollier, L. Chichet, B. Battelier, T. Lévèque, A. Landragin, and P. Bouyer, Dual matter-wave inertial sensors in weightlessness, Nat. Commun. **7**, 1 (2016).

[20] C. C. N. Kuhn, G. D. McDonald, K. S. Hardman, S. Bennetts, P. J. Everitt, P. A. Altin, J. E. Debs, J. D. Close, and N. P. Robins, A Bose-condensed, simultaneous dual-species Mach–Zehnder atom interferometer, New J. Phys. **16**, 073035 (2014).

[21] G. Rosi, G. D'Amico, L. Cacciapuoti, F. Sorrentino, M. Prevedelli, M. Zych, Č. Brukner, and G. M. Tino, Quantum test of the equivalence principle for atoms in coherent superposition of internal energy states, Nat. Commun. **8**, 1 (2017).

[22] P. W. Graham, D. E. Kaplan, J. Mardon, S. Rajendran, and W. A. Terrano, Dark matter direct detection with accelerometers, Phys. Rev. D **93**, 075029 (2016).

[23] M. Abe *et al.*, Matter-wave atomic gradiometer interferometric sensor (MAGIS-100), Quantum Sci. Technol. **6**, 044003 (2021).

[24] Baptiste Battelier *et al.*, Exploring the foundations of the physical universe with space tests of the equivalence principle, Exp. Astron. **51**, 1695 (2021).

[25] J. Li, G. R. M. da Silva, W. C. Huang, M. Fouda, J. Bonacum, T. Kovachy, and S. M. Shahriar, High sensitivity multi-axes rotation sensing using large momentum transfer point source atom interferometry, Atoms **9**, 51 (2021).

[26] J. M. McGuirk, M. J. Snadden, and M. A. Kasevich, Large Area Light-Pulse Atom Interferometry, Phys. Rev. Lett. **85**, 4498 (2000).

[27] K. Kotru, D. L. Butts, J. M. Kinast, and R. E. Stoner, Large-Area Atom Interferometry with Frequency-Swept Raman Adiabatic Passage, Phys. Rev. Lett. **115**, 103001 (2015).

[28] T. Kovachy, P. Asenbaum, C. Overstreet, C. A. Donnelly, S. M. Dickerson, A. Sugarbaker, J. M. Hogan, and M. A. Kasevich, Quantum superposition at the half-metre scale, Nature (London) **528**, 530 (2015).

[29] J. Rudolph, T. Wilkason, M. Nantel, H. Swan, C. M. Holland, Y. Jiang, B. E. Garber, S. P. Carman, and J. M. Hogan, Large Momentum Transfer Clock Atom Interferometry on the 689 nm Intercombination Line of Strontium, Phys. Rev. Lett. **124**, 083604 (2020).

[30] H. Müller, S. W. Chiow, S. Herrmann, and S. Chu, Atom Interferometers with Scalable Enclosed Area, Phys. Rev. Lett. **102**, 240403 (2009).

[31] P. Cladé, S. Guellati-Khélifa, F. Nez, and F. Biraben, Large Momentum Beam Splitter Using Bloch Oscillations, Phys. Rev. Lett. **102**, 240402 (2009).

[32] S. W. Chiow, T. Kovachy, H. C. Chien, and M. A. Kasevich, $102\hbar\kappa$ Large Area Atom Interferometers, Phys. Rev. Lett. **107**, 130403 (2011).

[33] G. D. McDonald, C. C. Kuhn, S. Bennetts, J. E. Debs, K. S. Hardman, M. Johnsson, J. D. Close, and N. P. Robins, $80\hbar$ k momentum separation with Bloch oscillations in an optically guided atom interferometer, Phys. Rev. A **88**, 053620 (2013).

[34] T. Mazzoni, X. Zhang, R. Del Aguila, L. Salvi, N. Poli, and G. M. Tino, Large-momentum-transfer Bragg interferometer with strontium atoms, Phys. Rev. A **92**, 053619 (2015).

[35] M. Kitagawa and M. Ueda, Squeezed spin states, Phys. Rev. A **47**, 5138 (1993).
[36] M. H. Schleier-Smith, I. D. Leroux, and V. Vuletić, Squeezing the collective spin of a dilute atomic ensemble by cavity feedback, Phys. Rev. A **81**, 021804 (2010).
[37] I. D. Leroux, M. H. Schleier-Smith, and V. Vuletić, Implementation of Cavity Squeezing of a Collective Atomic Spin, Phys. Rev. Lett. **104**, 073602 (2010).
[38] Y. L. Zhang, C. L. Zou, X. B. Zou, L. Jiang, and G. C. Guo, Detuning-enhanced cavity spin squeezing, Phys. Rev. A **91**, 033625 (2015).
[39] A. S. Sørensen and K. Mølmer, Entangling atoms in bad cavities, Phys. Rev. A **66**, 022314 (2002).
[40] B. K. Malia, *Integration of Spin Squeezed States into Free Space Atomic Sensors* (Stanford University, 2021).
[41] B. K. Malia, Y. Wu, J. Martínez-Rincón, and M. A. Kasevich, Distributed quantum sensing with mode-entangled spin-squeezed atomic states, Nature (London) **612**, 661 (2022).
[42] J. Li, G. R. da Silva, S. Kain, and S. M. Shahriar, Generalized echo squeezing protocol with near-Heisenberg-limit sensitivity and strong robustness against detection noise and variation in squeezing parameter, Phys. Rev. A **107**, 032610 (2023).
[43] R. Fang, R. Sarkar, and S. M. Shahriar, Enhancing the sensitivity of an atom interferometer to the Heisenberg limit using increased quantum noise, J. Opt. Soc. Am. B **37**, 1974 (2020).
[44] R. Sarkar, R. Fang, and S. M. Shahriar, High-Compton-frequency, parity-independent, mesoscopic Schrödinger-cat-state atom interferometer with Heisenberg-limited sensitivity, Phys. Rev. A **98**, 013636 (2018).
[45] J. Li, G. R. da Silva, S. Kain, G. Pati, R. Tripathi, and S. M. Shahriar, Spin-squeezing-induced enhancement of the sensitivity of an atomic clock using coherent population trapping, Phys. Rev. A **106**, 013112 (2022).
[46] E. Davis, G. Bentsen, and M. Schleier-Smith, Approaching the Heisenberg Limit Without Single-Particle Detection, Phys. Rev. Lett. **116**, 053601 (2016).
[47] O. Hosten, R. Krishnakumar, N. J. Engelsen, and M. A. Kasevich, Quantum phase magnification, Science **352**, 1552 (2016).
[48] M. Kasevich and S. Chu, Atomic Interferometry Using Stimulated Raman Transitions, Phys. Rev. Lett. **67**, 181 (1991).
[49] K. Moler, D. S. Weiss, M. Kasevich, and S. Chu, Theoretical analysis of velocity-selective Raman transitions, Phys. Rev. A **45**, 342 (1992).
[50] L. Salvi, N. Poli, V. Vuletić, and G. M. Tino, Squeezing on Momentum States for Atom Interferometry, Phys. Rev. Lett. **120**, 033601 (2018).
[51] One way to see why $\varphi + \varphi'$ will be cancelled is to consider the case where the acceleration-induced phase shift is zero. In this case, whatever the value of $\varphi + \varphi'$ is, the atoms will return to the initial state eventually, due to the implementation of the inverse of the first two steps. It is also obvious that an acceleration-induced phase shift cannot change $\varphi + \varphi'$ from being irrelevant to relevant.
[52] A. Peters, K. Y. Chung, and S. Chu, High-precision gravity measurements using atom interferometry, Metrologia **38**, 25 (2001).
[53] M. Kasevich and S. Chu, Laser Cooling Below a Photon Recoil with Three-Level Atoms, Phys. Rev. Lett. **69**, 1741 (1992).
[54] F. J. Harris, On the use of windows for harmonic analysis with the discrete Fourier transform, Proc. IEEE **66**, 51 (1978).
[55] G. Gabrielse, X. Fei, L. A. Orozco, R. L. Tjoelker, J. Haas, H. Kalinowsky, T. A. Trainor, and W. Kells, Thousandfold Improvement in the Measured Antiproton Mass, Phys. Rev. Lett. **65**, 1317 (1990).